Eng. Sci., 2025, **35**, 1535

Engineered Science
DOI: https://dx.doi.org/10.30919/es1535

Highly Efficient Florfenicol Removal via Nitrogen-Doped Zero-Valent Iron/Carbon Composites Activated with Peroxodisulfate: Mechanisms and Pathways

Peng Yu, Shun Wang, Xin Chen, Zhiguo Wang, Chun Zhang, Yanxue Shang and Wei Huang*

Abstract

Florfenicol (FF) accumulation in aquatic environments is a critical concern due to ecosystem disruption, microbial resistance, and health risks. While zero-valent iron (ZVI) is recognized for antibiotic remediation, studies on FF removal using nitrogen-doped ZVI-based materials activated by peroxodisulfate (PDS) and their degradation mechanisms are limited. This study synthesizes N-doped ZVI/C-1 via pyrolysis of iron-based metal-organic frameworks (MOFs), where organic ligands form a carbon matrix supporting ZVI particles and incorporate nitrogen atoms. The resulting N-doped ZVI/C-1 exhibits increased defect density, higher specific surface area, and improved hydrophobicity compared to ZVI/C. Electrochemical analyses further reveal that N-doped ZVI/C-1 possesses superior corrosion resistance, faster charge transport, and reduced hydrogen evolution activity. Consequently, N-doped ZVI/C-1 achieves a high FF removal efficiency of 96.0% within 30 minutes when activated by PDS. Mechanistic investigations indicate that the dominant degradation involves the generation of •OH and $•SO_4^-$ radicals, resulting in higher dechlorination and defluorination capacities compared to ZVI/C. Identified degradation pathways include C-Cl and C-F bond cleavage, C=O addition, and benzene ring decomposition, leading to a gradual reduction in FF toxicity. This study presents a promising strategy for FF removal and enhances the understanding of degradation mechanisms utilizing nitrogen-doped ZVI-based materials.

Keywords: Florfenicol; Nitrogen doping; Zero-valent iron; Removal mechanism.
Received: 31 March 2025; Revised: 19 May 2025; Accepted: 25 May 2025.
Article type: Research article.

1. Introduction

The use of antibiotics has increased significantly with advancements in medicine, agriculture, and animal husbandry.[1] Florfenicol (FF), a commonly used antibiotic,[2] plays a vital role in livestock management.[3] However, 45-60 % of the administered FF is excreted unchanged into the environment, primarily through animal urine.[4] FF has been detected in various natural environments, including water, soil, and sediments, with concentrations reaching up to 11 mg/L in coastal waters near Dalian, China.[5-7] Its chemical stability, due to inert C-F and C-Cl bonds, makes FF highly resistant to degradation and difficult to remove using conventional water treatment techniques.[8] The accumulation of FF disrupts aquatic ecosystems, fosters microbial resistance,[9] and poses health risks such as gastrointestinal toxicity and immune dysfunction in humans.[10] Consequently, the development of effective and sustainable FF removal technologies is critical for protecting ecosystems and public health.[11]

Various methods have been explored for removing FF from water bodies, including physical adsorption,[5] biodegradation,[12] and chemical oxidation.[13] Among these, advanced oxidation processes (AOPs) have received significant attention for their high efficiency.[14] AOPs are a promising technology capable of degrading organic pollutants through highly reactive free radicals, such as hydroxyl and sulfate radicals.[15] The design of catalysts is a critical factor in advanced oxidation technologies, as it directly influences the efficiency of the reactions. For example, Wang *et al.* achieved 84% FF degradation in 60 minutes using Co_3O_4-activated peroxymonosulfate (PMS).[16] Similarly, Wu *et al.* reported a 95% FF removal efficiency under alkaline conditions using a copper-based metal-organic framework with the addition of PMS.[17] However, the use of heavy-metal catalysts raises concerns about secondary contamination due to metal ion leaching.[18] In comparison, zero-valent iron (ZVI) is a more

School of Chemistry and Materials Science, Hunan Agricultural University, Changsha, 410128, China
**Email:* weihua@hunau.edu.cn (W. Huang)

environmentally friendly and cost-effective material for antibiotic removal, though it faces challenges such as passivation, oxidation, aggregation, and hydrogen evolution reactions.[19-21] To address these limitations, researchers have enhanced ZVI by compositing it with carbon materials, increasing porosity, stability, and active site density.[22] Additionally, doping ZVI with elements such as sulfur or nitrogen has improved its properties for FF removal.[23] For instance, Zhang *et al*. used sulfurized nano-ZVI loaded onto biochar for effective FF degradation.[24] Similarly, Tang and co-workers combined nitrogen-doped biochar with ZVI and zero-valent copper, leveraging experimental and density functional theory (DFT) methods to analyze degradation pathways.[25] Therefore, it is probable to utilize nitrogen doping as a crucial role to modulate the electronic structure, enhancing surface active sites, and promoting the corrosion resistance of ZVI, inhibits hydrogen evolution reactions, thus enhancing the removal capability of FF.[26]

Metal-organic frameworks (MOFs) and their derivatives are also promising materials for antibiotic removal due to their large surface area, tunable pore size, and versatile structures.[27] Metal-organic frameworks (MOFs) and their derivatives are also promising materials for antibiotic removal due to their large surface area, tunable pore size, and versatile structures.[28] For example, Zhu *et al*. achieved 82.6% ciprofloxacin removal using copper-loaded MOF-derived carbon materials.[29] Yu and co-workers demonstrated a 92% removal rate of norfloxacin using Co, Zn-MOF-derived Co@C-NCNTs activated by PMS.[30] Recent advancements in iron-based MOFs have shown potential for converting iron matrices into ZVI while transforming organic ligands into carbon layers embedded with ZVI.[31,32] Organic ligands containing nitrogen atoms can also introduce nitrogen dopants, altering the structural and chemical properties of the composites. However, studies on FF removal using such materials remain scarce, and the underlying mechanisms are not well understood. Developing novel nitrogen-doped ZVI/carbon composites as efficient catalysts is vital to overcoming current technological limitations and achieving effective FF removal.

In this study, nitrogen-doped ZVI/carbon composites are synthesized and systematically characterized. Comprehensive degradation experiments are conducted to evaluate its performance in FF removal. The effects of various operational parameters on removal efficiency are assessed, and potential reaction mechanisms are proposed. The findings underscore the significant potential of nitrogen-doped ZVI/carbon composites in environmental remediation, offering a sustainable, cost-effective, and innovative solution for FF removal.

2. Experimental section

2.1 Chemical reagents

All reagents were of analytical grade unless otherwise noted. Ferric chloride hexahydrate ($FeCl_3·6H_2O$,≥99.0%), 1,4-benzenedicarboxylic acid (H_2BDC, ≥99.0%), potassium persulfate (PDS, $K_2S_2O_8$, ≥99.5%), N, N-dimethylformamide(DMF, ≥99.5%) and methanol (CH_3OH, ≥99.5%) were sourced from Sinopharm Chemical Reagent Co., Ltd. (Shanghai, China), 2-methylimidazole (2-MI, ≥98.0%) was obtained from Guangfu Fine Chemical Research Institute (Tianjin, China), florfenicol (FF, ≥98.0%) was obtained from Macklin Biochemical Co., Ltd. (Shanghai, China).

2.2 Synthesis of N-doped ZVI/C composites

N-doped ZVI/C composites were synthesized by a typical method. First, solution A was prepared by dissolving H_2BDC (1.86 mmol) and 2-MI at molar ratios of 1:4 and 1:6 in 45 mL of DMF solution, respectively. Simultaneously, $FeCl_3·6H_2O$ (3.75 mmol) was dissolved in 15 mL of DMF to form solution B. solution A and solution B were then combined and transferred to a 150-mL polytetrafluoroethylene (PTFE) liner within an autoclave. The mixture was heated at 110 °C for 20 h. Afterwards, the resulting solid product was collected by centrifugation, washed thoroughly (at least three times), and dried. These preliminary products were subsequently annealed at 800 °C under an inert atmosphere for 3 h. The final samples were labeled as N-doped ZVI/C-1 and N-doped ZVI/C-2, corresponding to molar ratios of 1:4 and 1:6, respectively. As a control, pristine ZVI/C composite was synthesized following the same protocol but without adding 2-MI.

2.3 Characterization

X-ray diffractograms of synthetic materials were obtained by a D8 Advance X-ray diffractometer (XRD, SHIMADZLI 6000, Japan). The contact angle with water was determined by an optical contact angle meter (LAUDA Scientific LSA100, Germany). The surface functional groups were determined by Fourier transform infrared spectroscopy (FTIR, Bruker ALPHA, Germany). The surface chemical features of carbon in the materials were determined by a Raman chromatography analyzer (DXR300, Thermo Fisher Scientific). The specific surface area and porous structure were analyzed by the Brunauer-Emmett-Teller (BET, JW-BK100, China) method. The morphology and microstructure of synthesized materials were determined by electron microscopy (SEM, SU8600, 10 kV, Hitachi, Tokyo, Japan) and transmission electron microscopy (TEM, FEI Tecnai G2F 20), and the corresponding elemental composition and distribution were measured by the energy dispersive X-ray spectroscopy (EDS). X-ray photoelectron spectroscopy (XPS, Thermo Scientific K-Alpha, US) was performed to characterize the surface chemical valence states. The active species (•OH and $•SO_4^-$) were identified using electron paramagnetic resonance (EPR, Bruker EMXplus-6/1, Germany) with 5,5-diethyl-1-pyrroline N-oxide (DMPO) and 2,2,6,6-tetramethylpiperidine-1-oxyl (TEMP) as spin-trap reagents.

2.4 Batch experiments

All experiments for FF removal were performed in a 100-mL conical flask containing 50 mL of FF simulated wastewater.

The initial pH (pH_0) value of the solution was adjusted by 0.1 M NaOH or 0.1 M HCl. In a typical test, 10 mg of synthesized samples and 3 mM PDS were added to the flask for the removal of FF. The data was collected and analyzed at various time intervals (0, 5, 10, 15, 20, 30, 40, 60, and 120 min). Besides, the critical effect factors including the pH_0 (3, 4, 5, 6, 7, and 8), the dosage of PDS (0.5, 1, 3, 5, and 10 mM), the dosage of synthetic materials (5, 10, 15, and 20 mg), and the concentration of FF (20, 30, 40, and 50 mg/L), were systematically performed to analyze the removal behavior of FF. The FF concentration was determined by high-performance liquid chromatography (HPLC) at 224 nm. Each separation was performed on an Agilent C18 column (4.6 124 mm×150 mm×5 μm, Poroshell 120 HILIC) with a mobile phase of methanol and ultrapure water in a volume ratio of 38:62. The experiments were repeated thrice to ensure accuracy. Additionally, FF removal was tested in two real water samples: tap water and Liuyang River water, to evaluate performance under actual conditions. The degradation products of florfenicol (FF) were analyzed using a liquid mass spectrometer (UPLC-Zeno TOF 7600) operating in positive ion mode with a scan range of 0–500 m/z. The detailed batch experiment analysis method was provided in Test S1. The effects of coexisting ions and quenching experiments were shown in Text S2. Electrochemical analyses and measurements of iron, fluorine, and chlorine ions during degradation are detailed in Texts S3 and S4, respectively.

3. Results and discussion

3.1 Characterization of synthetic materials

The crystal structures of synthesized materials were analyzed using XRD. The diffraction peaks at 44.7° and 65.0° in the XRD spectra of ZVI/C, N-doped ZVI/C-1 (Fig. 1a), and N-doped ZVI/C-2 (Fig. S1) are in good agreement with the typical (110) and (200) facets of Fe^0 (JCPDS 87-0721).[33] Besides, the small diffraction peaks at 43.4° and 74.4° in the XRD spectrum of N-doped ZVI/C-1 align with the (111) and (220) crystalline facets of FeN (JCPDS 75-2128), suggesting the successful incorporation of nitrogen, originating from the nitrogen-containing organic ligands (2-MI).[34]

FTIR was used to identify the surface functional groups of ZVI/C and N-doped ZVI/C-1 (Fig. 1b). The bands observed at 584, 3440, 1580, and 1265 cm^{-1} are associated with the stretching vibrations of Fe-O, O-H, C=O, and C-O groups, respectively.[35] These results reveal that oxygen-containing functional groups, inherited from the original organic ligands, are present on the surfaces of both materials.[36] Raman spectroscopy (Fig. 1c) was employed to analyze the carbon features in ZVI/C and N-doped ZVI/C-1. The D and G bands represent disordered and graphitized carbon, respectively. The I_D/I_G ratio of N-doped ZVI/C-1 (0.986) is higher than that of ZVI/C (0.907). The more vacancies and defects in N-doped ZVI/C-1, the more active sites are available for the subsequent removal of FF.[37]

The specific surface areas (SSAs) of ZVI/C (Fig. 1d) and N-doped ZVI/C-1 (Fig. 1e) were subsequently assessed using adsorption-desorption isotherms. Both materials exhibit type IV isotherms, indicating mesoporous characteristics.[38] N-doped ZVI/C-1 (Table S1) has a significantly higher SSA (150.3 m^2/g) compared to ZVI/C (92.0 m^2 /g) and a higher

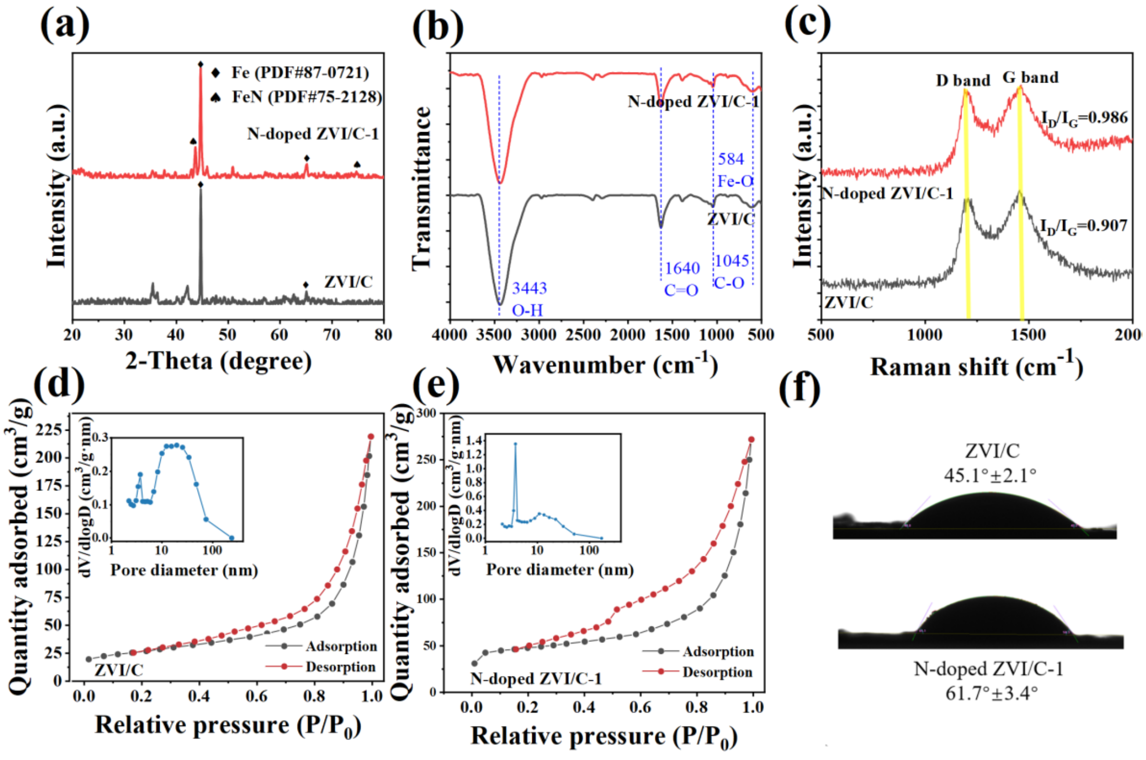

Fig. 1: XRD (a), FTIR (b) and Raman (c) spectra of ZVI/C and N-doped ZVI/C-1. Adsorption-desorption isotherms and corresponding pore-size distributions of ZVI/C (d) and N-doped ZVI/C-1 (e). (f) Contact angles of ZVI/C and N-doped ZVI/C-1.

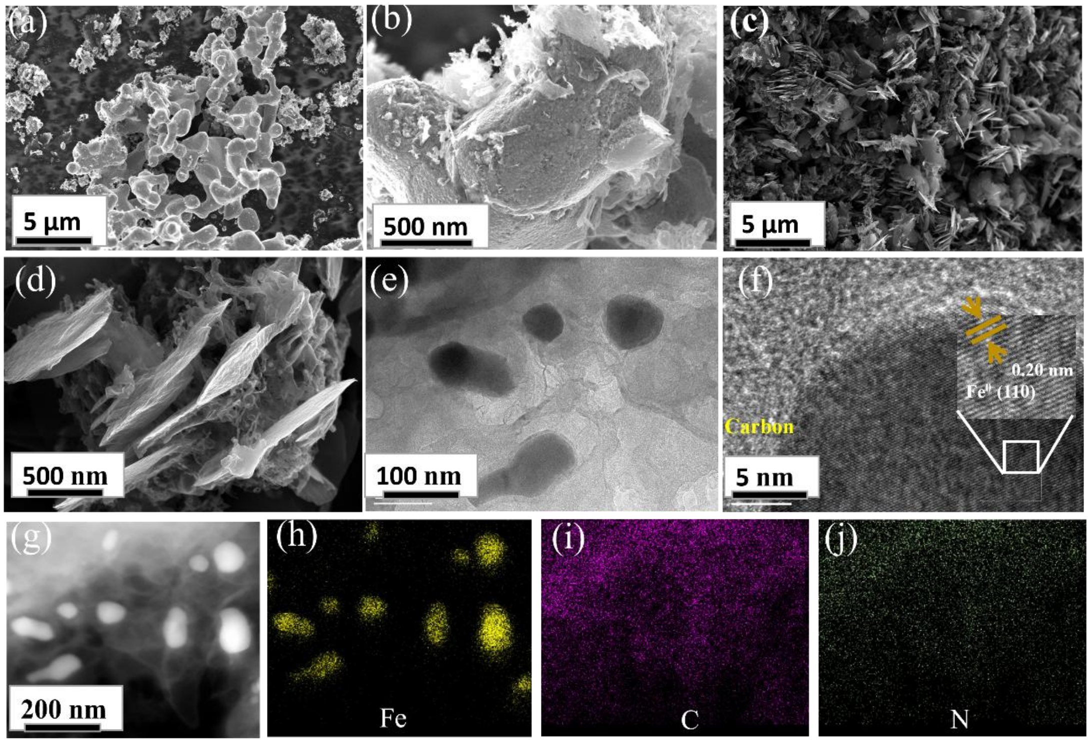

Fig. 2: SEM images of ZVI/C (a and b) and N-doped ZVI/C-1 (c and d). (e) TEM image of N-doped ZVI/C-1, (f) High-resolution TEM image of N-doped ZVI/C-1, inset is the lattice fringes of ZVI. HAADF-STEM image of N-doped ZVI/C-1 (g) and the corresponding EDS mapping of Fe (h), C (i) and N (j).

pore volume (0.41 cm^3/g versus 0.32 cm^3/g). The average pore size of N-doped ZVI/C-1 (10.8 nm) is smaller than that of ZVI/C (13.8 nm). These results indicate that the modification of nitrogen improves the SSA of N-doped ZVI/C-1 and refines the pore volume and average pore size efficiently. Besides, contact angle measurements (Fig. 1f) reveal that N-doped ZVI/C-1 (61.7° ± 3.4°) is more hydrophobic than ZVI/C (45.1° ± 2.1°), suggesting that N-doped ZVI/C-1 is more prone to interact with organic substances in solution.[39,40]

SEM images of ZVI/C (Figs. 2a and 2b) and N-doped ZVI/C-1 (Figs. 2c and 2d) highlight the superior dispersion and reduced aggregation of N-doped ZVI/C-1. These structural improvements increase the availability of reactive active sites for FF removal. SEM-EDS mapping results of N-doped ZVI/C-1 (Fig. S2) further indicate the uniform distribution of C, O, N and Fe elements. Besides, the TEM image of N-doped ZVI/C-1 (Fig. 2e) demonstrates that the Fe particles are uniformly dispersed into the carbon layers, and the lattice fringes shown in the high-resolution TEM image (Fig. 2f) possess a facet spacing of 0.20 nm, which corresponds to the (110) facet of Fe^0.[41] The size distribution of ZVI in N-doped ZVI/C-1 is determined to be 110.54±46 nm. Meanwhile, the high-angle annular dark-field-scanning TEM (HAADF-STEM) image (Fig. 2g) and corresponding mapping results further verify ZVI particles are embedded into nitrogen-doped carbon layers with a clear distribution of Fe (Fig. 2h), C (Fig. 2i) and N (Fig. 2j) elements in the composite.

The elemental compositions and chemical states of ZVI/C and N-doped ZVI/C-1 were characterized by XPS. The survey spectra (Fig. S3) confirm the presence of the elements C, O, and Fe in both materials, while the nitrogen signal is observed in the spectrum of N-doped ZVI/C-1, indicating the successful introduction of nitrogen elements in the N-doped ZVI/C-1. In the Fe 2p spectrum (Fig. 3a), the characteristic peaks of Fe(II) and Fe(III) are observed at 710.51/723.82 eV and 712.90/726.16 eV,[42] respectively. These surface Fe(II) and Fe(III) species primarily originate from the partial oxidation of surface Fe^0.[43] Additionally, both ZVI/C and N-doped ZVI/C-1 exhibit a representative Fe^0 peak at 706.55 eV.[44] In the C 1s spectra (Fig. 3b), peaks at 286.59, 285.58, and 284.80 eV are assigned to C-O, C-OH, and C-C bonds,[45] respectively. The N 1s spectrum (Fig. 3c) reveals peaks at 401.18 and 398.48 eV, corresponding to N=C and N-C configurations, respectively.[46]

ZVI/C and N-doped ZVI/C-1 were further investigated by electrochemical characterization. N-doped ZVI/C-1 has a higher Tafel potential (-0.45 V) than ZVI/C (-0.60 V), indicating improved corrosion resistance (see Fig. 3d).[47] Meanwhile, the smaller the radius of curvature of the Nyquist plot, the smaller the resistance to charge transfer (Rct).[48] The value of Rct for N-doped ZVI/C-1 (Fig. 3e) is smaller than that of ZVI/C, which indicates that the charge transfer rate of N-doped ZVI/C-1 is faster. In addition, the overpotential of N-doped ZVI/C for the hydrogen evolution reaction is higher than that of ZVI/C, verifying that the N-doped ZVI/C-1 is more difficult to catalyze water molecules for the generation of hydrogen gas than ZVI/C. This observation may be due to the hydrophobicity effects of N-doped ZVI/C-1, in good

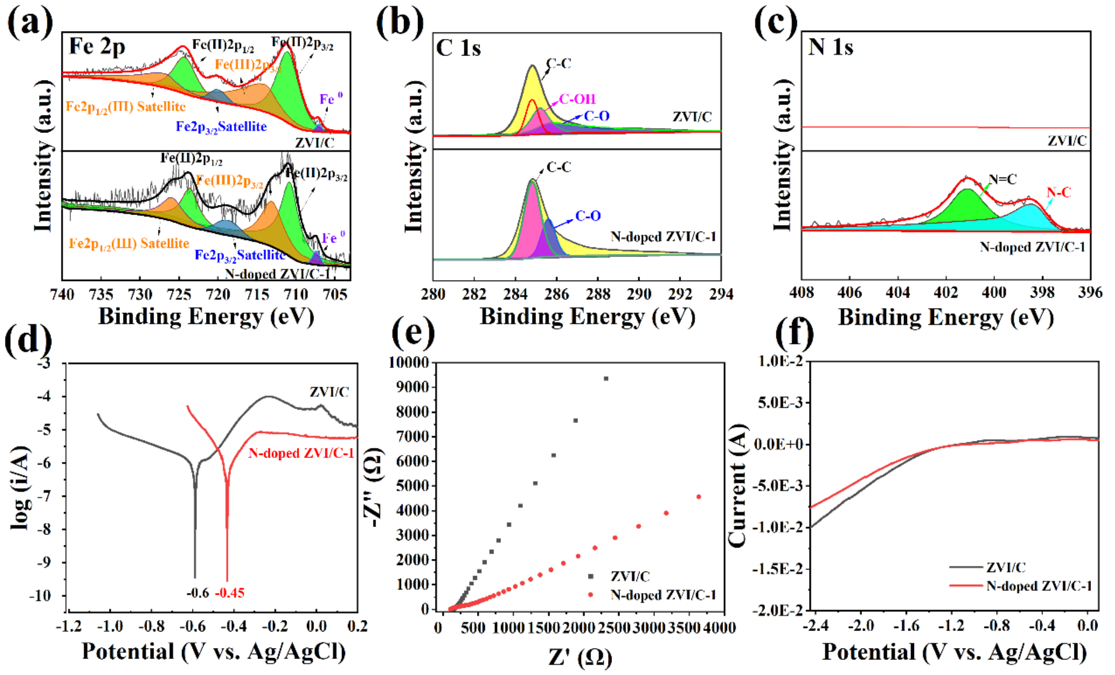

Fig. 3: Fe 2p (a), C 1s (b) and N 1s (c) spectra of ZVI/C and N-doped ZVI/C-1. Tafel scans (d), Nyquist plots (e) and LSV curves (f) of ZVI/C and N-doped ZVI/C-1.

agreement with the above result of contact angle (Fig. 1f), thus contributing to the removal of organic contaminants.

3.2 Removal behavior of FF

The synthetic materials (ZVI/C, N-doped ZVI/C-1 and N-doped ZVI/C-2) were used to investigate the removal behavior of FF. The removal capacities of FF (Fig. S4) with the addition of PDS are significantly higher compared to the materials without PDS or with pristine PDS. The removal efficiencies of FF (Fig. S5) via N-doped ZVI/C-1 and N-doped ZVI/C-2 without the assistance of PDS are 29.3% and 22.6%, respectively. This observation indicates that N-doped ZVI/C-1 and N-doped ZVI/C-2 could adsorb the partial FF molecules, the adsorbed FF molecules onto the materials is conducive to the efficient degradation of FF in the following experiments with the addition of PDS. The removal efficiencies (Fig. 4a) for ZVI/C, N-doped ZVI/C-1 and N-doped ZVI/C-2 with the assistance of PDS are 52.3%, 81.9% and 71.1%, respectively. The removal kinetics coefficient (Table S2) for N-doped ZVI/C-1 (0.09 min^{-1}) exceeds those of ZVI/C (0.07 min^{-1}) and N-doped ZVI/C-2 (0.06 min^{-1}), leading to the selection of N-doped ZVI/C-1 for further detailed analysis.

The critical effects of initial solution pH (pH$_0$), dosage of PDS, dosage of N-doped ZVI/C-1, and initial concentration of FF([FF]$_0$) upon FF removal by N-doped ZVI/C-1 were studied in detail. As shown in Fig. 4c, removal efficiencies of FF by N-doped ZVI/C-1 reach almost to 100% at pH$_0$ values of 3 and 4, with removal capacities (Fig. S6) of 141.4 and 136.5 mg/g, respectively. At pH$_0$ = 5, the removal efficiency is 88.8% with a capacity of 125.5 mg/g. A significant decline in efficiency is observed as pH$_0$ increases from 6 to 8. Thus, the pH$_0$ of 5 is selected for subsequent experiments. Besides, the effect of PDS dosage on FF removal is shown in Figs. 5d and S7. FF removal efficiencies are 61.8% and 85.5% at PDS dosages of 0.5 and 1 mM, respectively. When the PDS dosage is up to 3, 5 or 10 mM, the FF in the solution is removed completely within almost 10 min. With the cost consideration of PDS and better analysis of removal features of FF by N-doped ZVI/C-1, the PDS dosage of 1 mM is chosen for further studies. In addition, the suitable dosage of N-doped ZVI/C-1 (Figs. 4e and S8) is also considered in detail. The removal efficiencies of FF are 78.1%, 85.5%, 86.2%, and 91.2% at dosages of 5, 10, 15, and 20 mg, respectively. Since increasing the dosage beyond 10 mg results in only marginal gains, 10 mg is selected as the optimal dosage. Besides, removal efficiencies and capacities at different [FF]$_0$ are also shown in Figs. 4f and S9. At [FF]$_0$ values of 20, 30, 40, and 50 mg/L, removal efficiencies of FF are 96.1%, 85.5%, 70.1%, and 53.3%, respectively. Based on removal performance and environmental relevance, [FF]$_0$ = 20 mg/L is selected as the optimal concentration. Hence, the optimal conditions for FF removal are determined as pH$_0$ = 5, PDS dosage = 1 mM, N-doped ZVI/C-1 dosage = 10 mg, and [FF]$_0$ = 20 mg/L.

The impact of coexisting anions and cations on FF removal was also evaluated. As shown in Fig. 4g, removal efficiencies of FF decrease from 96.0% to 87.8%, 75.8%, 83.8%, 79.2%, and 87.4% with the addition of SO_4^{2-}, NO_3^{-}, $C0_3^{2-}$, PO_4^{3-}, and Cl^{-}, respectively SO_4^{-}(Table S3).[49] This observation indicates that there is only slight influence from the coexisting anions.[50] Meanwhile, When K^{+}, Ca^{2+}, Mg^{2+}, and Na^{+} ions are added into the solution, the removal efficiencies of FF decrease from 96.0% to 77.8%, 42.8%, 68.0%, and 87.4%, respectively, where the inhibition effect from Ca^{2+} is the greatest. The slight decrease in removal efficiency is mainly attributed to that the coexisting

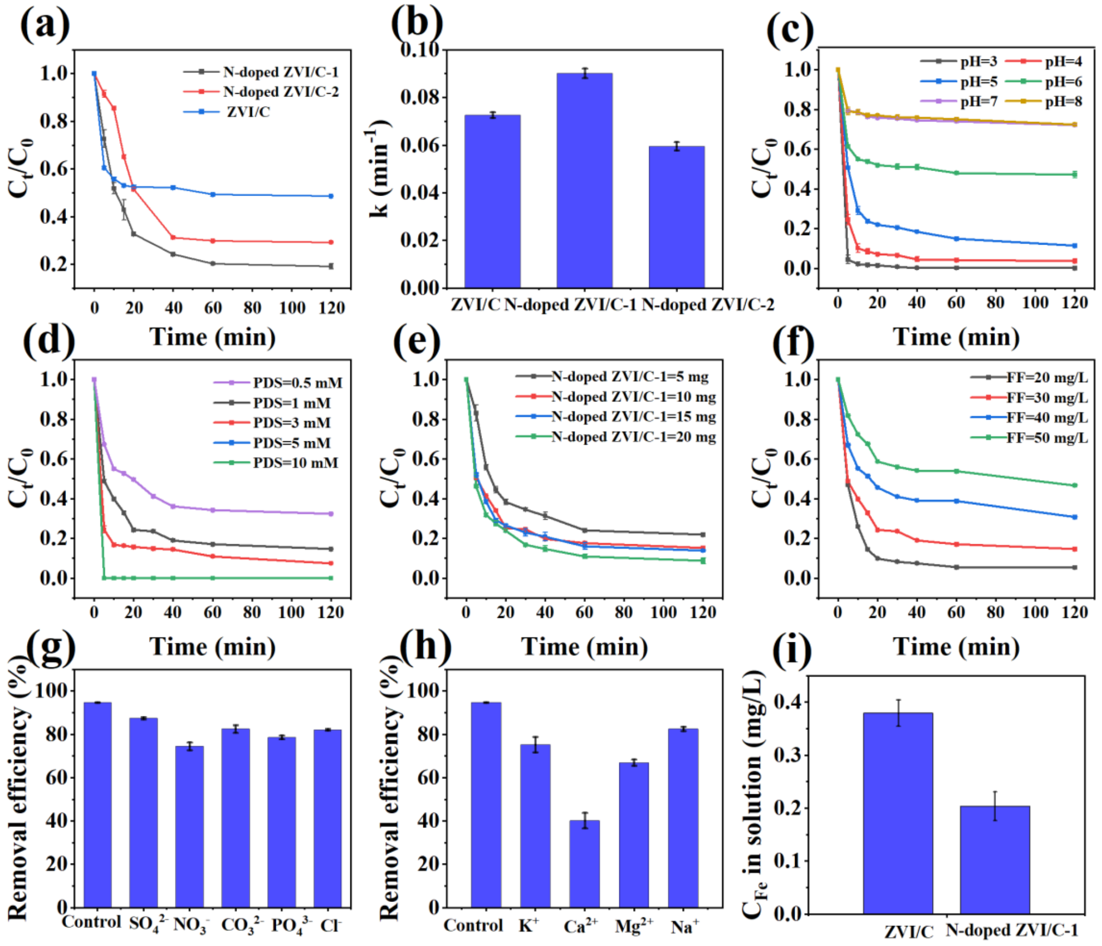

Fig. 4: Comparison of FF removal (a) and the corresponding removal kinetics coefficients (b) by ZVI/C, N-doped ZVI/C-1 and N-doped ZVI/C-2. Effects of pH_0 (c), dosage of PDS (d), dosage of N-doped ZVI/C-1 (e), and $[FF]_0$ (f) upon FF removal by N-doped ZVI/C-1. Competitive anions (g) and cations (h) upon FF removal by N-doped ZVI/C-1. (i) Fe leaching concentrations after reaction in ZVI/C and N-doped ZVI/C-1 systems.

K^+ and Mg^{2+} may compete with FF for adsorption onto the active sites on the N-doped ZVI/C-1 surface. This result would reduce the contact opportunity between FF and N-doped ZVI/C-1, thereby affecting the subsequent degradation of FF.[51] This is due to that Ca^{2+} ions would combine with SO_4^{2-} in the solution to form $CaSO_4$ particles, decreasing the availability of SO_4^{2-} in the solution, thus leading to the decay of removal capability of FF.

The Fe leaching concentrations after reaction in ZVI/C and N-doped ZVI/C-1 systems are shown in Fig. 4i, the Fe leaching concentration in the solution by N-doped ZVI/C-1 is 0.19 mg/L, much lower than that (0.39 mg/L) in ZVI/C systems. This result suggests that the introduction of N components improve the corrosion resistance of materials, thus reducing the risk of secondary pollution. Meanwhile, the Fe leaching concentration in the solution by N-doped ZVI/C-1 (0.19 mg/L) is lower than WHO suggested limit value for drinking water (≤ 0.3 mg/L), thus the N-doped ZVI/C-1 is enough safe for the FF removal. Further, N-doped ZVI/C-1 was tested for FF removal in real water samples (Fig. S10), including tap water and Liuyang River water. No significant FF contamination is detected in Tap water and Liuyang River water, The unadjusted-pH Tap water, Liuyang River water and with $[FF]_0$ of 20 mg/L are used for FF removal, with removal efficiencies of 77.11% and 77.6% respectively. This result highlights the potential applicability of N-doped ZVI/C-1 in real water.

3.3 Removal mechanism of FF

To elucidate the removal mechanism of FF by N-doped ZVI/C-1, XRD analysis of the material after the reaction (Fig. S11) reveals that the characteristic diffraction peaks of Fe^0 (JCPDS 87-0721) at 44.7° and 65.0° are preserved, indicating the structural stability of N-doped ZVI/C-1 during the process of FF removal. Furthermore, the SEM image and corresponding EDS results (Fig. S12) confirm the presence of Fe, Cl, F, C, N, and O elements. The Cl signal detected in the survey spectrum (Fig. S13a) after the reaction, along with the disappearance of the Fe^0 peak at 706.55 eV in the Fe 2p spectrum (Fig. S13b), suggests that surface Fe^0 components participate in the FF removal reaction.

Reactive oxygen species (ROS) involved in FF removal were investigated using quenching experiments (Fig. 5a). Tert-butanol (TBA), p-benzoquinone (P-BQ), methanol (MeOH),

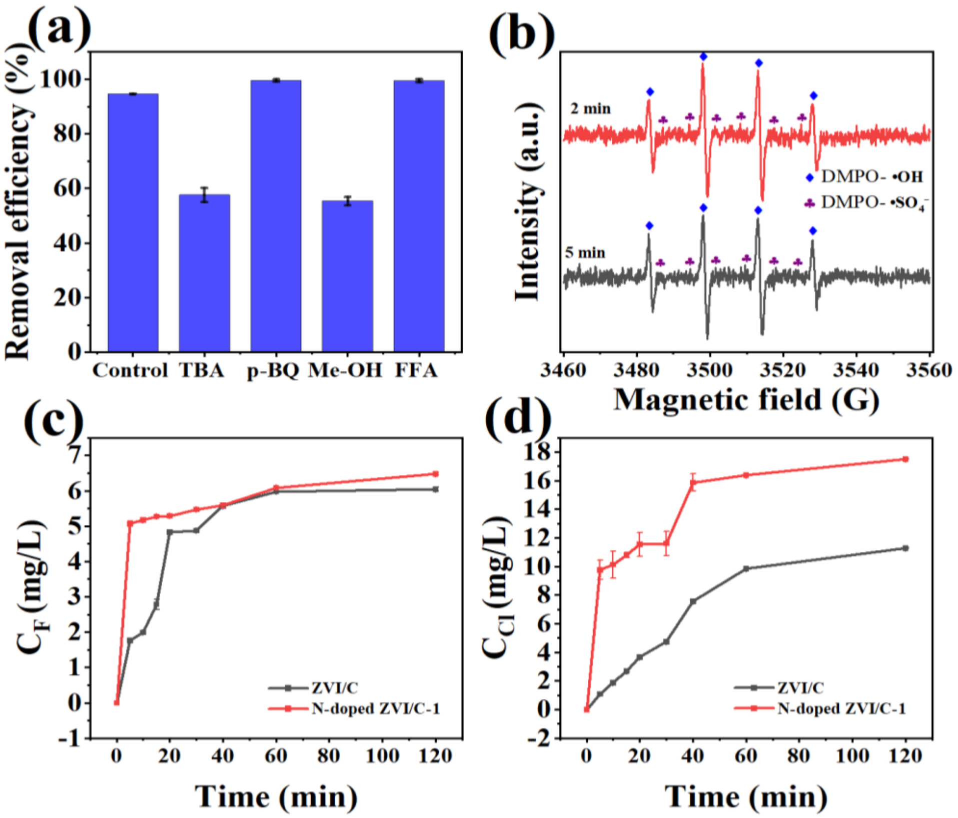

Fig. 5: (a) Effect of quenching agents upon FF removal efficiency. (b) EPR signals of DMPO-•OH and DMPO-•SO_4^-. The concentration changes of fluorine (c) and chlorine (d) ions in the solution during the removal process of FF. Experimental conditions: pH = 5, dosage = 10 mg, PDS= 1 mM, $[FF]_0$ = 20 mg/L, [TBA] = 30mM, [p-BQ] = 30 mM, [FFA] = 30 mM and [MeOH] = 30 mM.

and furfuryl alcohol (FFA) were employed to quench •OH, •O_2^-, •SO_4^-, and $^1O_2$, respectively. The results show that the addition of P-BQ and FFA has no significant effect on FF removal efficiency, whereas TBA and MeOH cause a marked decrease in FF removal. This indicates that •OH and •SO_4^- are the dominant ROS for FF degradation. Electron paramagnetic resonance (EPR) analysis (Fig. 5b) further confirms the presence of •OH and •SO_4^- radicals, which play a central role in the FF removal process by N-doped ZVI/C-1. The addition of TBA and MeOH, resulted in approximately a 50% reduction in FF removal efficiency. This finding indicates that while radical oxidation plays a significant role, other non-radical pathways also contribute to FF degradation. Specifically, control experiments performed without PDS (Fig. S5) demonstrate that N-doped ZVI/C-1 alone achieves a 29.3% FF removal efficiency, suggesting that adsorption contributes to the overall removal process. Furthermore, during the PDS-assisted reaction, the dissolution of ZVI could lead to the formation of iron ions on the surface of material. These surface-bound iron ions might act as coordination sites or bridges, potentially facilitating the complexation and subsequent removal or degradation of FF molecules.[52]

The concentration changes of fluorine (F^-) and chlorine (Cl^-) ions in solution during FF removal were monitored in Fig. 5c and 5d. The results indicate that the F^-concentration increases more rapidly in the N-doped ZVI/C-1 system compared to ZVI/C. Similarly, the Cl^- concentration also exhibits an increasing trend, with a higher final concentration (17.5 mg/L) in the N-doped ZVI/C-1 system compared to ZVI/C (11.3 mg/L). This demonstrates the superior dechlorination and defluorination ability of N-doped ZVI/C-1, confirming its enhanced efficiency in FF removal. Furthermore, Analysis of the solution following FF removal by N-doped ZVI/C-1 activated PDS reveal the presence of 6.48 mg/L fluoride ions (F^-) and 17.5 mg/L chloride ions (Cl^-). Since no external sources of F^- or Cl^- are introduced, these ions originate solely from the dehalogenation of FF molecules. Based on the detected fluoride concentration, it is determined that 32.4% of the removed FF molecules undergo defluorination and 43.7% of FF molecules are removed by dichlorination.

Furthermore, analysis of intermediate products using HPLC-MS indicates the formation of a product resulting from the cleavage of a single chloride ion. This observation suggests that some FF molecules undergo partial dechlorination during the reaction, while others may be fully dechlorinated. Considering the fluoride and chloride ion concentrations, along with the identification of a monochlorinated intermediate, the results collectively indicate selective dehalogenation of FF by the N-doped ZVI/C-1 activated PDS system, demonstrating selectivity in the removal of both fluorine and chlorine atoms.

The proposed removal mechanism (Fig. 6) involves the following reactions:

$$2S_2O_8^{2-} + Fe^0 \rightarrow 2 \bullet SO_4^- + Fe^{2+} + 2SO_4^{2-} \tag{1}$$

$$S_2O_8^{2-} + 2Fe^{2+} \rightarrow 2Fe^{3+} + 2SO_4^{2-} \tag{2}$$

$$\bullet SO_4^- + H_2O \rightarrow SO_4^{2-} + \bullet OH + H^+ \tag{3}$$

$$\bullet SO_4^- + OH^- \rightarrow SO_4^{2-} + \bullet OH \tag{4}$$

$$3Fe^0 + C_{12}H_{14}Cl_2FNO_4S + 3H^+ \rightarrow$$

$$3Fe^{2+} + C_{12}H_{17}NO_4S + 2Cl^- + F^- \tag{5}$$

$$FF + \cdot OH \rightarrow Intermediates \rightarrow CO_2 + H_2O + Products \tag{6}$$

The FF molecules are adsorbed onto the surface of N-doped ZVI/C-1, then peroxodisulfate reacts with zero-valent iron (Fe^0) to produce sulfate radicals ($\bullet SO_4^-$) and sulfate ions (SO_4^{2-}), with Fe^0 being oxidized to Fe^{2+} (Eq. 1). Fe^{2+} reacts further with peroxodisulfate to generate additional sulfate ions while being oxidized to Fe^{3+} (Eq. 2). Sulfate radicals ($\bullet SO_4^-$) react with water to produce hydroxyl radicals (•OH) and H^+, leading to a decrease in solution pH (Eq. 3). Additional hydroxyl radicals (•OH) are generated through the reaction of sulfate radicals with OH^- (Eq. 4). The hydroxyl radicals degrade FF by cleaving C-Cl and C-F bonds,[15] resulting in dechlorination and defluorination (Eq. 5),[53] FF are eventually decomposed by (•OH) attack into a series of intermediates and further mineralized to CO_2 and H_2O (Eq. 6), thus achieving effective FF removal.

3.4 Degradation products and toxicity analysis

HPLC-MS spectra (Fig. S14) were used to identify the degradation intermediates of FF. Several intermediates were detected, as presented in Fig. 7, and five potential degradation pathways for FF were proposed (Fig. 7a). In Pathway I, the C-F bond breaks, leading to the formation of a C=C bond, the cleavage of the C-OH bond to form a C=O group,[54] and the addition of -OH to the benzene ring, resulting in a final product.[55] Pathway II involves the cleavage of the C-F bond and the simultaneous formation of a C=C bond, along with the breaking of the C-site bond where -OH is located, producing a degradation product. Pathway III includes the cleavage of two C-Cl bonds, the C-F bond, and the C-S bond, generating the final product. Pathway IV entails the breaking of the C-Cl bond and the addition of -OH to the benzene ring, which forms the degradation product. Pathway V involves the formation of C=O, C=C=O, and C=C bonds, as well as the cleavage of the C-Cl and C=O bonds, resulting in the final product.

The potential toxicity of FF and its intermediates was assessed using the Toxicity Estimation Software Tool (T.E.S.T). The oral rat LD50, *Daphnia magna* lethality, and bioaccumulation factor (BAF) were evaluated (Figs. 7b-d). The results show that the oral rat LD50 of most intermediates decreases, except for intermediates C and G (Fig. 7b). *Daphnia magna* lethality also decreases for all intermediates except B and C, suggesting reduced ecological toxicity during degradation (Fig. 7c). Furthermore, the bioaccumulation factor values decrease for most intermediates (Fig. 7d), indicating reduced bioaccumulation potential and detoxification during FF degradation.[56] The results confirm that N-doped ZVI/C-1 effectively degrades FF while simultaneously reducing its toxicity.

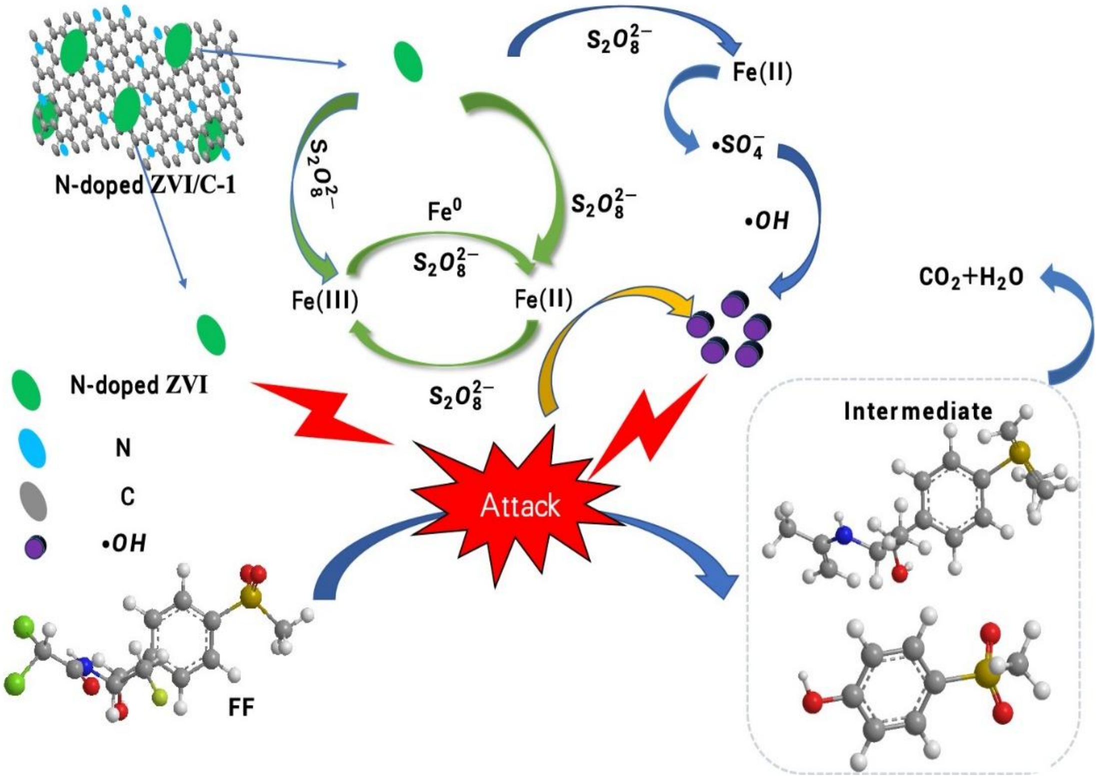

Fig. 6: Schematic illumination of removal mechanism of FF by N-doped ZVI/C.

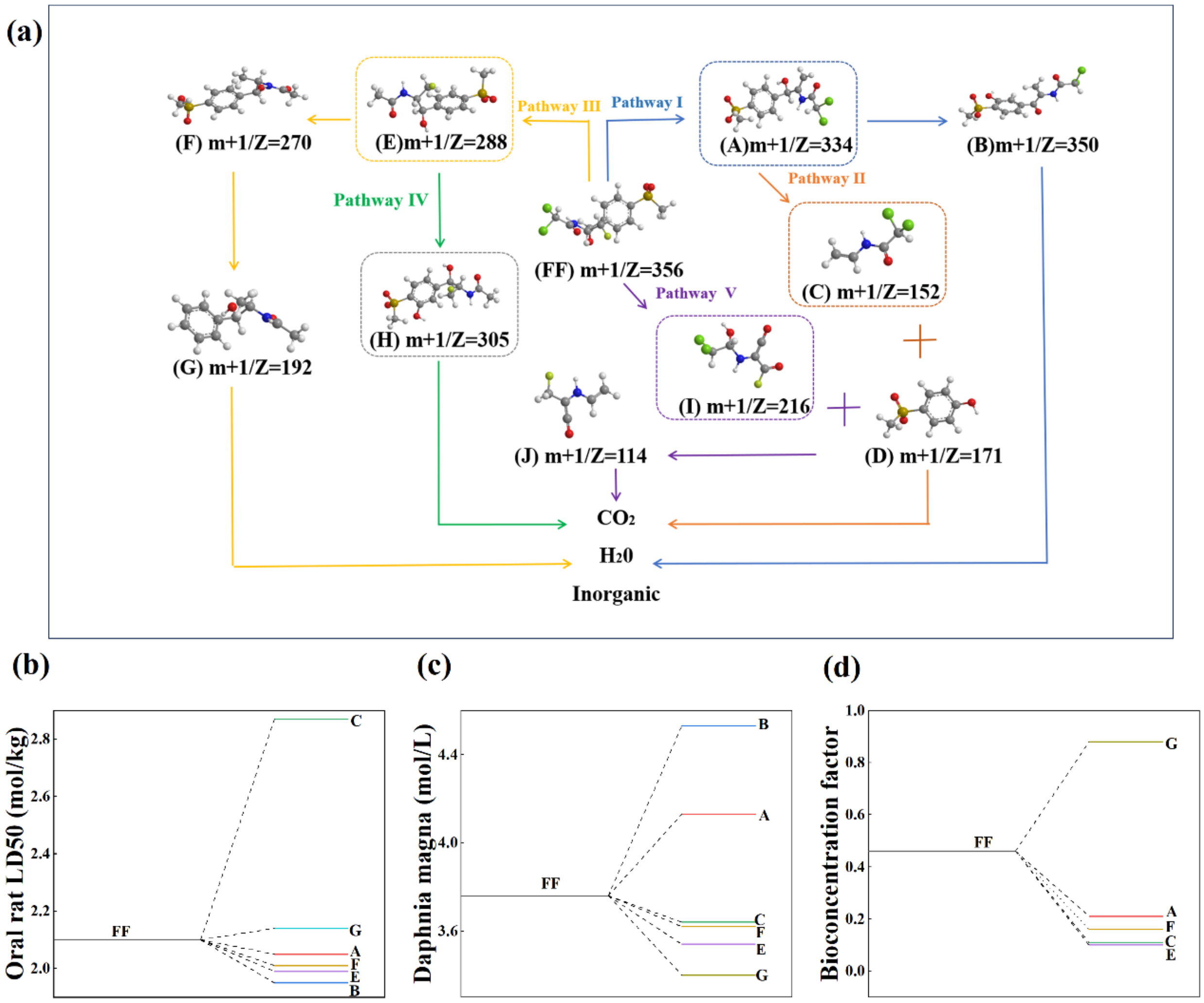

Fig. 7: Possible degradation pathways of FF (a), theoretically calculated Oral rat LD50 (b), daphnia magna (c), and bioaccumulation factor (d) of FF and its corresponding intermediates.

4. Conclusion

N-doped ZVI/C composites are successfully fabricated by pyrolyzing iron matrices and nitrogen-containing organic ligands from iron-based MOFs. The N-doped ZVI/C-1 possesses more defects, higher specific surface area and hydrophobicity than those of ZVI/C. Electrochemical analyses reveal that the N-doped ZVI/C-1 has superior corrosion resistance, faster charge transport and reduced hydrogen evolution activity compared to ZVI/C. These unique features of N-doped ZVI/C-1 significantly contribute to its effectiveness in FF removal, achieving a removal efficiency of 96.0% within 30 min in the presence of PDS. The removal mechanism of FF is primarily driven by •OH and $\bullet SO_4^-$, which are identified as the dominant reactive species. Furthermore, N-doped ZVI/C-1 demonstrates higher dechlorination and defluorination capacities than ZVI/C during FF removal. The degradation pathways of FF involve C-Cl and C-F bond cleavage, C=O addition, and benzene ring decomposition, accompany by a gradual reduction in toxicity throughout the process. This study offers a promising approach for the efficient removal of FF and advances the understanding of FF degradation mechanisms using nitrogen-doped ZVI-based materials with the assistance of PDS. However, further experimental validation is necessary to evaluate the application of this material for the removal of residual FF from soil.

Acknowledgements

This study was supported by the Project by Hunan Agricultural University for Supporting Young Interdisciplinary Scholars (2024XKJC03), Research Foundation of Education Bureau of Hunan Province, China (24A0150), Hunan Provincial Natural Science Foundation of China (2023JJ40330 & 2023JJ50322), Provincial Science and Technology Project of Nonggao District, Jinggangshan (20222-051245) and Postgraduate Scientific Research Innovation Project of Hunan Province (CX20240669).

Conflict of Interest

There is no conflict of interest.

Supporting Information

Applicable.

References

[1] G. Busch, B. Kassas, M. A. Palma, A. Risius, Perceptions of antibiotic use in livestock farming in Germany, Italy and the United States, *Livestock Science*, 2020, **241**, 104251, doi: 10.1016/j.livsci.2020.104251.

[2] A. S. Oliveira, M. Alves, F. Leitão, M. Tacão, I. Henriques, P. M. L. Castro, C. L. Amorim, Bioremediation of coastal aquaculture effluents spiked with florfenicol using microalgae-based granular sludge-a promising solution for recirculating aquaculture systems, *Water Research*, 2023, **233**, 119733, doi: 10.1016/j.watres.2023.119733.

[3] S. M. Mitchell, J. L. Ullman, A. L. Teel, R. J. Watts, Hydrolysis of amphenicol and macrolide antibiotics: chloramphenicol, florfenicol, spiramycin, and tylosin, *Chemosphere*, 2015, **134**, 504-511, doi: 10.1016/j.chemosphere.2014.08.050.

[4] M. Qiu, A. Hu, Y. M. Huang, Y. Zhao, Y. He, J. Xu, Z. Lu, Elucidating degradation mechanisms of florfenicol in soil by stable-isotope assisted nontarget screening, *Journal of Hazardous Materials*, 2021, **403**, 123974, doi: 10.1016/j.jhazmat.2020.123974.

[5] Y. He, C. Liu, X. Tang, Q. Xian, J. Zhang, Z. Guan, Biochar impacts on sorption-desorption of oxytetracycline and florfenicol in an alkaline farmland soil as affected by field ageing, *Science of The Total Environment*, 2019, **671**, 928-936, doi: 10.1016/j.scitotenv.2019.03.414.

[6] H. Zong, D. Ma, J. Wang, J. Hu, Research on florfenicol residue in coastal area of Dalian (northern China) and analysis of functional diversity of the microbial community in marine sediment, *Bulletin of Environmental Contamination and Toxicology,* 2010, **84**, 245-249, doi: 10.1007/s00128-009-9923-1.

[7] T. Chen, Z. Zhu, H. Zhang, X. Shen, Y. Qiu, D. Yin, Enhanced removal of veterinary antibiotic florfenicol by a Cu-based Fenton-like catalyst with wide pH adaptability and high efficiency, *ACS Omega*, 2019, **4**, 1982-1994, doi: 10.1021/acsomega.8b03406.

[8] Z. Zhao, W. Xie, Z. Huang, H. Cai, Y. Ji, B. Zhao, Investigation of the degradation and dehalogenation properties of florfenicol by heterogeneous Fenton reaction activated with MIL-53(Al)-supported nano zero-valent iron, *Chemical Engineering Journal*, 2023, **453**, 139420, doi: 10.1016/j.cej.2022.139420.

[9] M. Wang, X. Xie, M. Wang, J. Wu, Q. Zhou, Y. Sun, The bacterial microbiota in florfenicol contaminated soils: The antibiotic resistome and the nitrogen cycle, *Environmental Pollution*, 2020, **259**, 113901, doi: 10.1016/j.envpol.2019.113901.

[10] Y. Zhang, P. Guo, M. Wang, Y. Wu, Y. Sun, H. Su, J. Deng, Mixture toxicity effects of chloramphenicol, thiamphenicol, florfenicol in Daphnia Magna under different temperatures, *Ecotoxicology*, 2021, **30**, 31-42, doi: 10.1007/s10646-020-02311-3.

[11] J. Tang, Z. Li, X. Xiao, B. Liu, W. Huang, Q. Xie, C. Lan, S. Luo, L. Tang, Recent advancements in antibiotics removal by bio-electrochemical systems (BESs): From mechanisms to application of emerging combined systems, *Water Research*, 2025, **268**, 122683, doi: 10.1016/j.watres.2024.122683.

[12] C. Song, Y. Wei, Y. Qiu, Y. Qi, Y. Li, Y. Kitamura, Biodegradability and mechanism of florfenicol *via* chlorella sp. UTEX1602 and L38: experimental study, *Bioresource Technology*, 2019, **272**, 529-534, doi: 10.1016/j.biortech.2018.10.080.

[13] S. Periyasamy, X. Lin, S. O. Ganiyu, S. K. Kamaraj, A. Thiam, D. Liu, Insight into BDD electrochemical oxidation of florfenicol in water: Kinetics, reaction mechanism, and toxicity, *Chemosphere*, 2022, **288**, 132433, doi: 10.1016/j.chemosphere.2021.132433.

[14] M. Priyadarshini, I. Das, M. M. Ghangrekar, L. Blaney, Advanced oxidation processes: Performance, advantages, and scale-up of emerging technologies, *Journal of Environmental Management*, 2022, **316**, 115295, doi: 10.1016/j.jenvman.2022.115295.

[15] J. Scaria, P. V. Nidheesh, Comparison of hydroxyl-radical-based advanced oxidation processes with sulfate radical-based advanced oxidation processes, *Current Opinion in Chemical Engineering*, 2022, **36**, 100830, doi: 10.1016/j.coche.2022.100830.

[16] X. Wang, X. Luo, R. Li, Y. Chang, J. Peng, W. Wang, H. Liu, G. Yan, P. Wei, Z. Cao, Boosting peroxymonosulfate activation over partial Zn-substituted Co_3O_4 for florfenicol degradation: Insights into catalytic performance, degradation mechanism and routes, *Chemical Engineering Journal*, 2024, **491**, 152197, doi: 10.1016/j.cej.2024.152197.

[17] Y. Wu, G. Liang, W. Li, X. Zhong, Y. Zhang, J. Ye, T. Yang, Z. Mo, X. Chen, Boosting the degradation of antibiotics *via* peroxymonosulfate activation with a Cu-based metal-organic framework, *Chemical Science*, 2024, **15**, 9733-9741, doi: 10.1039/d4sc02850c.

[18] T. Hanawa, Metal ion release from metal implants, *Materials Science and Engineering: C*, 2004, **24**, 745-752, doi: 10.1016/j.msec.2004.08.018.

[19] X. Chen, D. Song, J. Xu, G. Sun, M. Xu, Microbial depassivation of Fe(0) for contaminant removal under semi-aerobic conditions, *Applied Microbiology and Biotechnology*, 2017, **101**, 8595-8605, doi: 10.1007/s00253-017-8549-1.

[20] S. Wei, C. He, L. Zhang, C. Li, J. Li, G. Du, Advancements in removing common antibiotics from wastewater using nano zero valent iron, *RSC Advances*, 2024, **14**, 26272-26291, doi: 10.1039/d4ra04336g.

[21] Z. Yang, J. Tang, H. Feng, X. Liu, X. Zhuang, H. Wang, Y. Wu, Y. Guo, L. Tang, Research progress on remediation of heavy metal contaminated soil by electrokinetic-permeable reactive barrier, *Chemical Engineering Journal*, 2024, **490**, 151548, doi: 10.1016/j.cej.2024.151548.

[22] J. Shi, J. Wang, W. Wang, W. Teng, W. Zhang, Stabilization of nanoscale zero-valent iron in water with mesoporous carbon (nZVI@MC), *Journal of Environmental Sciences*, 2019, **81**, 28-33, doi: 10.1016/j.jes.2019.02.010.

[23] Y. Xie, Q. Wang, Z. Guo, L. Qian, M. Chen, J. Yan, Electron induced efficient dechlorination of trichlorethylene with S doped Fe_2B: The enhancement mechanism of S, *Environment International*, 2022, **170**, 107619, doi:

10.1016/j.envint.2022.107619.

[24] J. Zhang, H. Yu, W. Xu, H. Shi, X. Hu, J. Xu, L. Lou, Adsorption-reduction coupling mechanism and reductive species during efficient florfenicol removal by modified biochar supported sulfidized nanoscale zerovalent iron, *Environmental Research*, 2023, **216**, 114782, doi: 10.1016/j.envres.2022.114782.

[25] Z. Tang, Y. Kong, Y. Qin, X. Chen, M. Liu, L. Shen, Y. Kang, P. Gao, Performance and degradation pathway of florfenicol antibiotic by nitrogen-doped biochar supported zero-valent iron and zero-valent copper: a combined experimental and DFT study, *Journal of Hazardous Materials*, 2023, **459**, 132172, doi: 10.1016/j.jhazmat.2023.132172.

[26] Y. Li, Z. Qu, C. Shan, Effects of sulfidation/nitridation on the reactivity of nanoscale zero-valent iron towards chlorinated organic compounds of different polarities, *Separation and Purification Technology*, 2024, **341**, 126916, doi: 10.1016/j.seppur.2024.126916.

[27] C. Du, Z. Zhang, G. Yu, H. Wu, H. Chen, L. Zhou, Y. Zhang, Y. Su, S. Tan, L. Yang, J. Song, S. Wang, A review of metal organic framework (MOFs)-based materials for antibiotics removal *via* adsorption and photocatalysis, *Chemosphere*, 2021, **272**, 129501, doi: 10.1016/j.chemosphere.2020.129501.

[28] Y. Liu, J. Wang, Z. Yin, Y. Ma, Y. Kou, W. Yang, Titanium metal organic framework based electrocatalytic membrane for fast antibiotics removal: Synergy of defects and hierarchical pore, *Separation and Purification Technology*, 2023, **323**, 124517, doi: 10.1016/j.seppur.2023.124517.

[29] S. Zhu, C. Sun, Z. Fang, M. Qin, Z. Zhu, J. Qu, H. Zheng, Copper-supported MOF-derived carbon materials for highly efficient antibiotics removal, *Journal of Environmental Chemical Engineering*, 2024, **12**, 113756, doi: 10.1016/j.jece.2024.113756.

[30] J. Yu, B. Hu, P. Nie, X. Shang, B. Zhang, Z. Tang, J. Yang, J. Liu, Co, Zn-MOF derived Co@C-NCNTs for boosting non-radical oxidation of norfloxacin by peroxymonosulfate, *Colloids and Surfaces A: Physicochemical and Engineering Aspects*, 2022, **647**, 129037, doi: 10.1016/j.colsurfa.2022.129037.

[31] Y. Li, W. Qin, S. Chen, T. Gu, Y. Chen, F. Pei, S. Li, F. Yu, Iron-based metal organic framework (Fe-MOF)-doped sesame stalk biochar enhances antibiotic degradation: Important role of free radicals and comparison of multiple degradation processes, *Separation and Purification Technology*, 2025, **353**, 128464, doi: 10.1016/j.seppur.2024.128464.

[32] R. Yin, Y. Chen, S. He, W. Li, L. Zeng, W. Guo, M. Zhu, *In situ* photoreduction of structural Fe(III) in a metal-organic framework for peroxydisulfate activation and efficient removal of antibiotics in real wastewater, *Journal of Hazardous Materials*, 2020, **388**, 121996, doi: 10.1016/j.jhazmat.2019.121996.

[33] Y. Fei, N. Han, J. Shi, S. Tang, H. Zhuang, L. Wang, J. Ran, E. Gao, M. A. Habila, Z. Chen, D. Tao, B. Ni, M. Jiang, Red mud-derived iron carbon catalyst for the removal of organic pollutants in wastewater, *Chemosphere*, 2023, **337**, 139211, doi: 10.1016/j.chemosphere.2023.139211.

[34] C. Feng, Y. Guo, S. Qiao, Y. Xie, L. Zhang, L. Zhang, W. Wang, J. Wang, 2-Methylimidazole as a nitrogen source assisted synthesis of a nano-rod-shaped Fe/FeN@N-C catalyst with plentiful FeN active sites and enhanced ORR activity, *Applied Surface Science*, 2020, **533**, 147481, doi: 10.1016/j.apsusc.2020.147481.

[35] M. Danish, X. Gu, S. Lu, A. Ahmad, M. Naqvi, U. Farooq, X. Zhang, X. Fu, Z. Miao, Y. Xue, Efficient transformation of trichloroethylene activated through sodium percarbonate using heterogeneous zeolite supported nano zero valent iron-copper bimetallic composite, *Chemical Engineering Journal*, 2017, **308**, 396-407, doi: 10.1016/j.cej.2016.09.051.

[36] P. Wiercik, B. Frączek, P. Chrobot, Fouling of anion exchanger by image and FTIR analyses, *Journal of Environmental Chemical Engineering*, 2020, **8**, 103761, doi: 10.1016/j.jece.2020.103761.

[37] J. Tan, R. Zhuang, S. Li, X. Chen, X. Xiao, J. Tang, Z. Wang, C. Zhang, Q. Wang, P. Yu, W. Huang, Efficient co-removal of aqueous Cr(VI) and ciprofloxacin by alkali lignin-derived carbon supported nanoscale zero-valent iron *via* adsorption and redox synergistic mechanisms, *Separation and Purification Technology*, 2025, **354**, 129402, doi: 10.1016/j.seppur.2024.129402.

[38] P. Yu, J. Tan, R. Zhuang, J. Tang, Z. Wang, C. Zhang, Q. Wang, X. Xiao, W. Huang, Valorization of heavy metals enriched ALB adsorbents as effective ZnS-CdS/C photocatalysts for antibiotics removal, *Journal of Alloys and Compounds*, 2024, **1002**, 175447, doi: 10.1016/j.jallcom.2024.175447.

[39] C. Xue, J. T. Lott, V. B. Kolachalama, Estimation of size and contact angle of evaporating sessile liquid drops using texture analysis, *Langmuir*, 2019, **35**, 3672-3679, doi: 10.1021/acs.langmuir.8b04043.

[40] L. Chen, X. Zhu, J. Yuan, R. Wang, J. Li, Y. Wang, Y. Peng, J. Li, Unveiling the role of hydrophobicity on multilayer carbon nanosheets enriched in sp^2-carbon for toluene adsorption under humid conditions, *Environmental Science & Technology*, 2024, **58**, 16175-16185, doi: 10.1021/acs.est.4c03365.

[41] T. Huang, G. Zhang, N. Zhang, J. Ye, P. Lu, Fe0-H_2O_2 for advanced treatment of citric acid wastewater: Detailed study of catalyst after several times use, *Chemical Engineering Journal*, 2018, **336**, 233-240, doi: 10.1016/j.cej.2017.11.147.

[42] S. Zhang, M. Wu, T. Tang, Q. Xing, C. Peng, F. Li, H. Liu, X. Luo, J. Zou, X. Min, J. Luo, Mechanism investigation of anoxic Cr(VI) removal by nano zero-valent iron based on XPS analysis in time scale, *Chemical Engineering Journal*, 2018, **335**, 945-953, doi: 10.1016/j.cej.2017.10.182.

[43] E. P. Arévalo-López, P. Romero-Moreno, J. L. Rosas-Huerta, L. Huerta, C. Minaud, M. L. Marquina, R. Escamilla, M. Romero, Effect of Fe on Bi_2Te_3: structure, magnetic properties, and XPS valence band, *Journal of Alloys and Compounds*, 2022, **899**, 163297, doi: 10.1016/j.jallcom.2021.163297.

[44] G. Sheng, A. Alsaedi, W. Shammakh, S. Monaquel, J. Sheng, X. Wang, H. Li, Y. Huang, Enhanced sequestration of selenite in water by nanoscale zero valent iron immobilization on carbon nanotubes by a combined batch, XPS and XAFS investigation, *Carbon*, 2016, **99**, 123-130, doi: 10.1016/j.carbon.2015.12.013.

[45] J. Chen, L. Cui, Y. Yan, X. Ji, Q. Fei, Y. Ma, *In situ* preparation of oriented microbial consortium-based compound enzyme strengthens food waste disintegration and anaerobic

digestion: Performance, mechanism, microbial communities and global metabolic pathways, *Chemical Engineering Journal*, 2024, **486**, 150208, doi: 10.1016/j.cej.2024.150208.

[46] X. Ren, Y. Chen, Y. Wang, H. Fu, D. Hu, X. Feng, Grafting modification of thin-film composite membrane with quaternary ammonium polyelectrolyte for Mg^{2+}/Li^{+} separation, *Journal of Environmental Chemical Engineering*, 2024, **12**, 112223, doi: 10.1016/j.jece.2024.112223.

[47] O. van der Heijden, S. Park, R. E. Vos, J. J. J. Eggebeen, M. T. M. Koper, Tafel slope plot as a tool to analyze electrocatalytic reactions, *ACS Energy Letters*, 2024, **9**, 1871-1879, doi: 10.1021/acsenergylett.4c00266.

[48] G. Nabi, A. Riaz, A. Dahshan, M. Tanveer, M. Maraj, W. Ali, Sn doping role in structural modifications and electrochemical performance of $Co(OH)_2$ nanorods for supercapacitors applications, *Materials Chemistry and Physics*, 2024, **314**, 128944, doi: 10.1016/j.matchemphys.2024.128944.

[49] W. Huang, Z. Yang, J. Hu, X. Chen, W. Li, Z. Wang, C. Zhang, Q. Wang, X. Xiao, P. Yu, Mechanisms and valorization of selective adsorption of Sb(III) by amino-functionalized lignin-based porous biochar, *Chemical Engineering Journal*, 2024, **499**, 156262, doi: 10.1016/j.cej.2024.156262.

[50] P. Yu, J. Xing, J. Tang, Z. Wang, C. Zhang, Q. Wang, X. Xiao, W. Huang, Polyethyleneimine-modified iron-doped birnessite as a highly stable adsorbent for efficient arsenic removal, *Journal of Colloid and Interface Science*, 2024, **661**, 164-174, doi: 10.1016/j.jcis.2024.01.163.

[51] Q. Zhou, W. Ju, Y. Yong, Q. Zhang, Y. Liu, J. Li, Effect of the N/P/S and transition-metal co-doping on the quantum capacitance of supercapacitor electrodes based on mono- and multilayer graphene, *Carbon*, 2020, **170**, 368-379, doi: 10.1016/j.carbon.2020.08.045.

[52] J. Kong, S. Gao, Y. Liu, X. Jin, D. Wei, S. Jiang, K. Ye, J. Wang, P. Xing, X. Luo, Recycling of carbonized rice husk for producing high purity silicon by the combination of electric arc smelting and slag refining, *Journal of Hazardous Materials*, 2019, **380**, 120827, doi: 10.1016/j.jhazmat.2019.120827.

[53] Y. Peng, C. Xue, J. Luo, B. Zheng, Z. Fang, Lanthanum-doped magnetic biochar activating persulfate in the degradation of florfenicol, *Science of The Total Environment*, 2024, **916**, 170312, doi: 10.1016/j.scitotenv.2024.170312.

[54] Y. Ding, Y. Zhu, X. Yu, S. Lyu, Y. Wu, L. Zhou, Q. Sui, Mechanistic and kinetic aspects of florfenicol degradation by OH: Chloride moiety resistance, *Chemical Engineering Journal*, 2024, **479**, 147696, doi: 10.1016/j.cej.2023.147696.

[55] Z. Chen, J. Chen, S. Tan, Z. Yang, Y. Zhang, Dechlorination helps defluorination: insights into the defluorination mechanism of florfenicol by S-nZVI and DFT calculations on the reaction pathways, *Environmental Science & Technology*, 2024, **58**, 2542-2553, doi: 10.1021/acs.est.3c07435.

[56] A. M. Gorito, A. R. L. Ribeiro, P. Rodrigues, M. F. R. Pereira, L. Guimarães, C. M. R. Almeida, A. M. T. Silva, Antibiotics removal from aquaculture effluents by ozonation: chemical and toxicity descriptors, *Water Research*, 2022, **218**, 118497, doi: 10.1016/j.watres.2022.118497.

Open Access